The Astrophysical Journal, 689:1161–1172, 2008 December 20

CORRELATIONS OF PROMPT AND AFTERGLOW EMISSION IN *SWIFT* LONG AND SHORT GAMMA-RAY BURSTS

N. Gehrels,[1] S. D. Barthelmy,[1] D. N. Burrows,[2] J. K. Cannizzo,[1,3] G. Chincarini,[4,5] E. Fenimore,[6] C. Kouveliotou,[7] P. O'Brien,[8] D. M. Palmer,[6] J. Racusin,[2] P. W. A. Roming,[2] T. Sakamoto,[1,3] J. Tueller,[1] R. A. M. J. Wijers,[9] and B. Zhang[10]

Received 2008 February 4; accepted 2008 August 21

ABSTRACT

Correlation studies of prompt and afterglow emission from gamma-ray bursts (GRBs) between different spectral bands have been difficult to do in the past because few bursts had comprehensive and comparable afterglow measurements. In this paper we present a large and uniform data set for correlation analysis based on bursts detected by the *Swift* mission. For the first time, short and long bursts can be analyzed and compared. It is found for both classes that the optical, X-ray, and gamma-ray emission are linearly correlated, but with a large spread about the correlation line; stronger bursts tend to have brighter afterglow, and bursts with brighter X-ray afterglow tend to have brighter optical afterglow. Short bursts are, on average, weaker in both prompt and afterglow emission. No short bursts are seen with extremely low optical–to–X-ray ratios, as occurs for "dark" long bursts. Although statistics are still poor for short bursts, there is no evidence yet for a subgroup of short bursts with high extinction, as there is for long bursts. Long bursts are detected in the dark category in the same fraction as pre-*Swift* bursts. Interesting cases of long bursts that are detected in the optical, and yet have a low enough optical–to–X-ray ratio to be classified as dark, are discovered. For the prompt emission, short and long bursts have different average tracks on flux versus fluence plots. In *Swift*, GRB detections tend to be fluence-limited for short bursts and flux-limited for long events.

Subject heading: gamma rays: bursts

1. INTRODUCTION

One of the longest enduring gamma-ray burst (GRB) classification schemes is based on their distributions in duration and spectral hardness. Both quantities seem to cluster into two separate classes, with the longer events (those above ~2 s; Kouveliotou et al. 1993) being predominantly softer while the shorter ones are harder. The mechanism for the origin of the GRB explosions (the central engine) appears to be quite different for the two types. Long bursts are ascribed to the core collapse to a black hole of a massive, young, rapidly rotating star in the "collapsar" model (Woosley 1993; MacFadyen & Woosley 1999; Woosley & Bloom 2006), which is supported by observations such as the coincidence of supernovae with well-observed nearby GRBs (Galama et al. 1998; Bloom et al. 1999; Stanek et al. 2003; Hjorth et al. 2003; Pian et al. 2006). The prevalent model for short bursts describes them as caused by the coalescence of a binary pair of compact old stars (Lattimer & Schramm 1974; Paczyński 1986; Eichler et al. 1989; Mochkovitch et al. 1993; Rosswog et al. 2003; Oechslin et al. 2007) and is supported by recent observations of progenitor sites with low star formation activity (Gehrels et al. 2005; Bloom et al. 2006; Fox et al. 2005; Villasenor et al. 2005; Hjorth et al. 2005; Barthelmy et al. 2005a; Berger et al. 2005). In both scenarios, a highly relativistic collimated outflow of particles and radiation occurs, producing prompt gamma-ray emission from shock-accelerated electrons, which evolves into a long-lasting afterglow from shock interactions with the circumburst medium (e.g., Mészáros & Rees 1997). For short bursts there are also models for the afterglow in which a radioactive wind causes emission in the first day or so (Li & Paczyński 1998; Kulkarni 2005).

Correlation studies of prompt and afterglow emission are crucial for understanding their production mechanisms and environmental effects. For example, Jakobsson et al. (2004) developed a criterion for determining which GRBs are "dark" bursts by comparing the relative intensity of their X-ray and optical afterglow to find what fraction of bursts have high column densities. Stratta et al. (2004) studied the X-ray and optical absorption properties of 13 GRBs studied by *BeppoSAX*. Roming et al. (2006) and Fynbo et al. (2007) expanded on previous work to include (long) bursts from the *Swift* satellite. More detailed work on dark bursts using a broadband spectral analysis is given by Rol et al. (2005, 2007). Zhang et al. (2007) present a study comparing radiative efficiencies for short and long bursts as derived from a correlation analysis. Using *Swift* short bursts, Berger (2007) compared their X-ray afterglow to their gamma-ray prompt emission and found that 20% have anomalously low X-ray–to–gamma-ray ratios, indicating very low density burst sites, possibly in globular clusters, for that subpopulation (see also Berger et al. 2007). Other correlation studies have been undertaken by Salmonson & Galama (2002), Firmani et al. (2006), Nava et al. (2006), Butler (2007), and

[1] NASA Goddard Space Flight Center, Greenbelt, MD 20771; neil.gehrels@nasa.gov.
[2] Department of Astronomy and Astrophysics, Pennsylvania State University, State College, PA 16802.
[3] CRESST/Joint Center for Astrophysics, University of Maryland, Baltimore County, Baltimore, MD 21250.
[4] INAF—Osservatorio Astronomico di Brera, 1-23807 Merate, Italy.
[5] Universita degli Studi di Milano Bicocca, 1-20126 Milano, Italy.
[6] Los Alamos National Laboratory, P.O. Box 1663, Los Alamos, NM 87545.
[7] NASA Marshall Space Flight Center, NSSTC, VP-62, 320 Sparkman Drive, Huntsville, AL 35805.
[8] Department of Physics and Astronomy, University of Leicester, Leicester LE1 7RH, UK.
[9] Faculty of Science, Astronomical Institute "Anton Pannekoek", University of Amsterdam, Kruislaan 403, 1098 SJ Amsterdam, Netherlands.
[10] Department of Physics and Astronomy, University of Nevada, Las Vegas, NV 89154.

Nysewander et al. (2008). An early study of X-ray afterglow properties at $t = 11$ hr was carried out by Piran et al. (2001).

In this paper we perform correlation studies using the extensive data set from *Swift*. Sections 2 and 3 cover observations and results, respectively, while in § 4 we discuss the implications of the results and in § 5 the conclusions and future prospects.

2. OBSERVATIONS

2.1. *Swift Studies*

The *Swift* mission (Gehrels et al. 2004) has so far provided *uniform observations of prompt and afterglow emission* for hundreds of GRBs. This sample is an order of magnitude larger than the one previously available with, e.g., the *BeppoSAX* satellite (de Pasquale et al. 2006).[11] Furthermore, *Swift* X-ray observations covering timescales from 1 minute to several days after the burst are provided for the first time for almost every GRB. After 3 yr of operations, our data set has now reached a critical size where statistically meaningful correlations can be studied.

We present here three correlation studies: (1) X-ray versus optical afterglow, (2) gamma-ray prompt versus X-ray afterglow, and (3) prompt gamma-ray peak flux versus fluence. All the data used in this study are listed in Tables 1–4, except that gamma-ray data are listed only for those bursts with at least an X-ray afterglow. The full list of fluences and fluxes for the 193 bursts used for study 3 are directly from the Sakamoto et al. (2008) tables. We include all *Swift* bursts from 2005 January through 2007 July for studies 1 and 2 and through 2007 February for study 3. We adopt $T90 = 2$ s for the dividing line between long and short GRBs, except for those with soft extended emission. In those cases the duration of the initial hard pulse is required to be <2 s, and only that emission is used in the analysis (GRB 050724, 051227, 061006, 061210, and 070714B). Including the extended emission in the fluence would increase it by a factor of $\lesssim 2$ and would not significantly change the correlations.

For the X-ray versus optical afterglow study, we use the methods developed by Jakobsson et al. (2004) in their comparison of X-ray and optical afterglow fluxes for pre-*Swift* bursts. In order to compare to the Jakobsson et al. results, we use the same definition of quantities: the X-ray flux density at 3 keV, the optical flux in the *R* band, and the sampling time at 11 hr after the burst. The *Swift* X-ray light curves have been typically found to have complex shapes (Nousek et al. 2006; Zhang et al. 2006), often including a poorly understood "plateau phase"; the use of flux at 11 hr in most cases avoids sampling during the plateau phase and gives a measure of the true burst afterglow.

2.2. *X-Ray Fluxes*

The X-ray fluxes are from measurements of the *Swift* X-Ray Telescope (XRT; Burrows et al. 2005). Our primary data product for the XRT flux is the integral flux between 0.3 and 10 keV corrected for absorption at low energies (unabsorbed flux). This is converted to the flux density at 3 keV using the measured spectral index. Given an integral 0.3–10 keV X-ray flux $[I_X] =$ erg cm^{-2} s^{-1} and a 0.3–10 keV X-ray photon index n, the flux density at 3 keV, in μJy, is given by

$$f_X(3\ \mathrm{keV}) = 4.13 \times 10^{11}\, \frac{I_X(2-n)E_0^{1-n}}{\left(E_2^{2-n} - E_1^{2-n}\right)}, \qquad (1)$$

where $E_0 = 3$, $E_1 = 0.3$, and $E_2 = 10$ keV.

[11] See also the Web site by J. Greiner, http://www.mpe.mpg.de/~jcg/grbgen.html.

The integral fluxes, photon spectral indices, and flux densities are listed in Tables 1–3. A 10% systematic uncertainty was added in quadrature to the measured error to account for uncertainties in the shape and variability of the light curves. The integral flux calculation was carried out as follows (see J. Racusin et al. [2008, in preparation] for a more detailed discussion of the method). Level 1 data products were downloaded from the NASA/GSFC *Swift* Data Center (SDC) and processed using XRTDAS software (ver. 2.0.1). The `xrtpipeline` task was used to generate level 2 cleaned event files. Only events with windowed timing (WT) mode grades 0–2, photon counting (PC) mode grades 0–12, and energies between 0.3 and 10.0 keV were used in subsequent temporal and spectral analysis.

The XRT light curves were created by extracting the counts in a circular region around the GRB afterglow with a variable source radius designed to optimize the signal-to-noise ratio, depending on the count rate. They were background-subtracted and pileup-corrected where applicable, exposure map–corrected, and corrected for the fraction of the PSF excluded by the extraction region. The number of counts per bin was variable and dependent on the count rate. Time intervals of significant flaring were removed from the light curves and fit to power laws, broken power laws, and multiply broken power laws. Using these temporal fits, we interpolated the count rate at 11 hr.

Spectra for the power-law segments of the light curves were extracted individually to limit contamination by potential spectral variability. The segment used for the counts-to-flux conversion was that at 11 hr. The spectra were created by extracting the counts in a 20 pixel radius extraction region and a 40 pixel radius background region. The ancillary response files were made using the `xrtmkarf` task and grouped with 20 counts per bin using the `grppha` task. The spectra were fit in XSPEC to absorbed power laws and used to measure the 0.3–10 keV flux and count rate, which was applied to the interpolated count rate to convert into flux units.

2.3. *Optical and Gamma-Ray Fluxes*

The optical fluxes are from measurements by ground-based telescopes and the *Swift* UV Optical Telescope (UVOT; Roming et al. 2005). An extensive literature search was done to find the best optical data for each burst. Bursts were included in the study if measurements were available within a factor of 2 of 11 hr (i.e., at >5.5 or <22 hr). The value at 11 hr was estimated by interpolations and extrapolations when measurements were not available at exactly 11 hr. The correction applied to the *R* data for $t_{\rm obs} \neq 11$ hr was $\Delta m_R = -2.5 \log_{10}(t_{\rm obs}/11\ \mathrm{hr})$. The one exception to the factor of 2 criterion was GRB 070508, with measurements to only 4 hr, which was included because it appears to be an interesting dark burst candidate. A few bursts are listed with optical flux upper limits at the bottom of Table 2. This is not an exhaustive list of optical limits, but only those with low optical–to–X-ray ratio limits. A 10% systematic uncertainty was added in quadrature to the measured error to account for uncertainties in the shape and variability of the light curves.

Galactic extinction was taken into account using the study of Schlegel et al. (1998).[12] For the precise sky map positions we used the XRT localizations. For each data source reference, a determination had to be made as to whether the galactic correction had already been made. (For the GCN entries, it was always assumed that the correction had not been made.) For most of the GRBs, the *R*-band correction was small (a few tenths of a magnitude). The exceptions from Table 1 are 050724 ($\Delta m_R = 1.64$)

[12] See http://nedwww.ipac.caltech.edu/forms/calculator.html.

TABLE 1

Swift Short GRBs with X-Ray or Optical Data at 11 hr

GRB	γ-Ray Fluence[a] (10^{-7} erg cm^{-2})	γ-Ray Fluence Error[a] (10^{-7} erg cm^{-2})	X-Ray Integral Flux, 0.3–10 keV @11 hr (10^{-13} erg cm^{-2} s^{-1})	X-Ray Integral Flux Error[b] (10^{-13} erg cm^{-2} s^{-1})	X-Ray Spectrum Photon Index	X-Ray Spectrum Photon Index Lower Error	X-Ray Spectrum Photon Index Upper Error	X-Ray[b] Flux Density @3 keV @11 hr (10^{-3} μJy)	X-Ray[b] Flux Density Error (10^{-3} μJy)	m_R	m_R Error	Time[c] *R*-Band Data or Code (hr)	*R* Flux Density[d] @11 hr (μJy)	*R* Flux Density Error (μJy)	*R* Ref.
050509B.....	0.09	0.02	...	...	...	...	...	...	...	>21.9	UL	11.0	<5.0	UL	1
050724.....	9.98	1.2	1.59	0.51	2.06	0.52	0.79	6.03	2.6	20.3	0.2	Ff	23.6	4.4	2
050813.....	0.44	0.11	...	...	...	...	...	...	...	>22.5	UL	13.0	<3.1	UL	3
051220.....	0.85	0.14	...	...	...	...	...	...	...	...	...	...	...	...	...
051221A.....	11.5	0.35	7.52	1.4	2.12	0.17	0.19	27.5	6.9	21.9	0.5	If	5.22	2.5	4
051227.....	6.99	1.1	0.864	0.18	1.86	0.21	0.23	3.63	0.93	24.9	0.12	11.45	0.333	0.04	5
060313.....	11.3	0.45	4	0.66	2.27	0.2	0.23	13	3.6	>20.6	UL	8.4	<17.2	UL	6
060502B.....	0.4	0.05	...	...	...	...	...	...	...	>23.2	UL	16.8	<1.54	UL	7
060801.....	0.8	0.1	<0.139	UL	2.69	0.69	1.1	<0.297	UL	...	...	...	...	...	...
061006.....	14.2	1.4	1.66	0.43	1.78	0.28	0.44	7.17	2.3	21.8	0.2	14.6	6.0	1.1	8
061201.....	3.34	0.27	2.07	0.59	1.61	0.27	0.55	9.32	3	22.7	0.3	8.38	2.52	0.7	9
061217.....	0.42	0.07	2.17	3.1	...	...	...	...	...	...	...	...	...	...	...
070724A.....	0.3	0.07	1.18	0.53	2.1	0.46	0.57	4.34	2.7	...	...	...	...	...	...
070729.....	1	0.2	0.16	0.091	2.11	0.77	1.5	0.586	0.5	...	...	...	...	...	...
070809.....	1	0.1	4.55	1.5	1.4	0.35	0.5	20.8	7.6	23.8	0.2	11.21	0.879	0.16	10

[a] BAT prompt fluence in 15–150 keV band. Data from Sakamoto et al. (2008).

[b] XRT flux at 3 keV at 11 hr after the burst trigger. The error includes 10% systematic uncertainty.

[c] Hours after burst trigger of optical data or code for optical data. If a number, it is the time after the burst (typically listed for GCN-only data). If letters, the capital letters are as follows: F, full light curve; I, interpolated between measured values on either side of 11 hr; and E, extrapolated from measured data. The lowercase letters indicate whether the data in the referenced papers were in magnitudes or Janskys (mmf = first two references in magnitudes, third reference in Janskys).

[d] Optical data in the *R* band at 11 hr after the burst trigger. The *R*-band flux is estimated from typical burst spectra if data were taken in other bands. The error includes 10% systematic uncertainty.

References.—(1) Misra & Pandey 2005; (2) Malesani et al. 2007a; (3) Bikmaev et al. 2005; (4) Soderberg et al. 2006; (5) Berger et al. 2007; (6) Schmidt & Bayliss 2006; (7) Price et al. 2006; (8) Malesani et al. 2006; (9) D'Avanzo et al. 2006; (10) Perley et al. 2007.

TABLE 2

Swift Long GRBs with X-Ray and Optical Detections or Low Upper Limits at 11 hr

GRB	γ-Ray Fluence[a] (10^{-7} erg cm^{-2})	γ-Ray Fluence Error[a] (10^{-7} erg cm^{-2})	X-Ray Integral Flux 0.3–10 keV @11 hr (10^{-13} erg cm^{-2} s^{-1})	X-Ray Integral Flux Error[b] (10^{-13} erg cm^{-2} s^{-1})	X-Ray Spectrum Photon Index	X-Ray Spectrum Photon Index Lower Error	X-Ray Spectrum Photon Index Upper Error	X-Ray Flux Density[b] @3 keV @11 hr (10^{-3} μJy)	X-Ray Flux Density Error[b] (10^{-3} μJy)	m_R	m_R Error	Time *R*-Band Data or Code[c] (hr)	*R* Flux Density[d] @11 hr (μJy)	*R* Flux Density Error (μJy)	*R* Ref.
With OPT @11 hr															
050315.....	32.2	1.5	41.9	3.2	2	0.068	0.071	165	16	20.7	0.2	11.6	16.4	3	1
050318.....	10.8	0.77	9.61	1.4	1.93	0.13	0.14	39.2	7.3	20.2	0.2	Ef	26	4.8	2
050319.....	13.1	1.5	45	9.6	2.05	0.12	0.13	171	45	20.2	0.1	Fmmmf	25	2.3	3, 4, 5, 6
050416A.....	3.67	0.37	10.4	1.3	2.1	0.12	0.14	38.5	6.5	21.2	0.1	Fff	9.94	0.92	7, 8
050525A.....	153	2.2	14.3	2.7	2.32	0.2	0.26	44.8	14	19.6	0.1	Ffmf	43.4	4	9, 10, 2
050721.....	36.2	3.2	12.7	1.6	1.93	0.15	0.2	51.7	8.9	21.4	0.6	If	8.27	4.8	11
050730.....	23.8	1.5	62.8	3.3	1.72	0.051	0.052	277	17	20.2	0.1	Fmff	25.8	2.4	12, 13, 2
050801.....	3.1	0.48	2.47	0.66	1.85	0.18	0.28	10.4	3.3	21.5	0.3	Ef	7.54	2.1	14
050802.....	20	1.6	15.4	1.7	1.84	0.087	0.094	65.2	8.7	20.7	0.2	Ff	15.1	2.8	2
050820A.....	34.4	2.4	176	7.5	2.02	0.048	0.049	681	40	18.8	0.1	Ffff	87.2	8	13, 15, 2
050824.....	2.66	0.52	9.88	3.6	2.01	0.22	0.24	38.7	17	21.2	0.2	Ff	9.94	1.8	16
050908.....	4.83	0.51	1.24	0.38	1.88	0.28	0.45	5.15	2	21.9	0.5	If	5.06	2.4	2
050922C.....	16.2	0.54	8.27	1.5	2.15	0.18	0.19	29.5	7.5	20.8	0.3	7	14.3	4	17
051109A.....	22	2.7	48.5	6.4	2.02	0.13	0.14	189	33	19.7	0.1	Fff	39.6	3.7	18, 2
060108.....	3.69	0.37	6	1.5	2.08	0.25	0.29	22.5	7.6	22.5	0.4	If	3	1.1	19
060124.....	4.61	0.53	223	16	2.04	0.078	0.081	856	83	19.1	0.1	Fmf	68.8	6.3	20, 2
060206.....	8.31	0.42	18.6	2.4	2.23	0.14	0.16	62.6	13	18.9	0.1	Fffff	82.7	7.6	21, 22, 23, 2
060210.....	76.6	4.1	106	5.3	2.13	0.057	0.058	383	28	23.4	0.1	Fmf	1.37	0.13	24, 2
060418.....	83.3	2.5	5.12	1.9	2.24	0.59	0.96	17.1	12	20.2	0.1	Ff	25	2.3	13
060512.....	2.32	0.4	2.98	1.1	2.19	0.35	0.53	10.3	5.8	21.1	0.16	6.8	10.5	1.6	25
060526.....	12.6	1.6	8.69	1.7	1.74	0.17	0.24	38	9	19.7	0.1	Fmf	39.6	3.7	26, 2
060604.....	4.02	1.1	11.5	2.1	2.07	0.17	0.19	43.2	11	20.6	0.2	16.5	17.2	3.2	27
060605.....	6.97	0.9	4.36	1	2.1	0.19	0.27	16.1	5	20.6	0.2	Ff	17.8	3.3	2
060607A.....	25.5	1.1	23.8	3.4	1.59	0.13	0.14	108	18	20.4	0.3	Ef	20.8	5.8	28
060614.....	204	3.6	70.3	11	2.04	0.15	0.16	269	55	19.2	0.1	Ffmf	62.7	5.8	29, 30, 2
060714.....	28.3	1.7	9.18	1.6	2.18	0.17	0.18	32.2	7.8	21.1	0.15	8.7	11.3	1.6	31
060729.....	26.1	2.1	218	16	2.1	0.076	0.078	805	84	16.6	0.18	20	716	120	32
060904B.....	16.2	1.4	5.57	0.87	2.22	0.17	0.18	18.9	4.5	20.2	0.2	15.7	25.9	4.8	33
061007.....	444	5.6	11.3	0.11	1.78	0.014	0.014	48.7	0.63	21	0.2	Im	12	2.2	34
061021.....	29.6	1	37.5	2.7	2.08	0.079	0.083	140	14	19.5	0.1	16.5	49	4.5	35
061110A.....	10.6	0.76	0.845	0.31	1.95	0.32	0.41	3.41	1.5	23	0.3	8	1.98	0.55	36
061121.....	137	2	82	8.4	1.84	0.1	0.11	347	44	20.1	0.1	Fff	27.4	2.5	37, 2
061126.....	67.7	2.2	33.2	2.4	1.95	0.096	0.1	133	13	21.4	0.1	Fm/f	8.27	0.76	38
070224.....	3.05	0.51	2.49	1.1	2.1	0.67	0.91	9.2	6.3	23.4	0.3	7.2	1.37	0.38	39
070419B.....	73.6	2	204	16	1.68	0.092	0.096	906	85	22.8	0.2	7.3	2.38	0.44	40
070508.....	196	2.7	32.1	1.2	1.7	0.054	0.057	142	6.5	23.3	0.2	4.1	1.48	0.27	41
070518.....	1.62	0.24	1.87	0.7	2.27	0.5	0.68	6.12	4	22.7	0.2	9	2.52	0.47	42

TABLE 2—*Continued*

GRB	γ-Ray Fluence[a] (10^{-7} erg cm^{-2})	γ-Ray Fluence Error[a] (10^{-7} erg cm^{-2})	X-Ray Integral Flux 0.3–10 keV @11 hr (10^{-13} erg cm^{-2} s^{-1})	X-Ray Integral Flux Error[b] (10^{-13} erg cm^{-2} s^{-1})	X-Ray Spectrum Photon Index	X-Ray Spectrum Photon Index Lower Error	X-Ray Spectrum Photon Index Upper Error	X-Ray Flux Density[b] @3 keV @11 hr (10^{-3} μJy)	X-Ray Flux Density Error[b] (10^{-3} μJy)	m_R	m_R Error	Time *R*-Band Data or Code[c] (hr)	*R* Flux Density[d] @11 hr (μJy)	*R* Flux Density Error (μJy)	*R* Ref.
Optical Limit @11 hr															
050713B.....	31.8	3.2	77.5	12	1.89	0.17	0.19	321	65	>24.6	UL	6	<2.72	UL	43
061004.....	5.66	0.31	2.06	0.67	2.4	0.53	0.67	6.04	4.2	>24.5	UL	12	<5.86	UL	44
061222A.....	79.9	1.6	158	13	2.09	0.095	0.099	587	68	>26.1	UL	16	<1.69	UL	45
070721A.....	0.71	0.18	1.43	0.45	2.65	0.39	0.39	3.17	2.1	>26.6	UL	18.8	<1.33	UL	46

[a] BAT prompt fluence in 15–150 keV band. Data from Sakamoto et al. (2008).

[b] XRT flux at 3 keV at 11 hr after the burst trigger. The error includes 10% systematic uncertainty.

[c] Hours after burst trigger of optical data or code for optical data. If a number, it is the time after the burst (typically listed for GCN-only data). If letters, the capital letters are as follows: F, full light curve; I, interpolated between measured values on either side of 11 hr; and E, extrapolated from measured data. The lowercase letters indicate whether the data in the referenced papers were in magnitudes or Janskys (mmf = first two references in magnitudes, third reference in Janskys).

[d] Optical data in the *R* band at 11 hr after the burst trigger. The *R*-band flux is estimated from typical burst spectra if data were taken in other bands. The error includes 10% systematic uncertainty.

REFERENCES.—(1) Cobb & Bailyn 2005; (2) Liang et al. 2008; (3) Woźniak et al. 2005; (4) George et al. 2006; (5) Huang et al. 2007; (6) Kamble et al. 2007; (7) Ghirlanda et al. 2007; (8) Soderberg et al. 2007; (9) Shao & Dai 2005; (10) Della Valle et al. 2006; (11) Antonelli et al. 2006; (12) Pandey et al. 2006; (13) Chen et al. 2007; (14) Rykoff et al. 2006; (15) Cenko et al. 2006; (16) Sollerman et al. 2007; (17) Durig & Price 2005; (18) Yost et al. 2007; (19) Oates et al. 2006; (20) Misra et al. 2007; (21) Monfardini et al. 2006; (22) Stanek et al. 2007; (23) Curran et al. 2007a; (24) Curran et al. 2007b; (25) Milne 2006; (26) Dai et al. 2007; (27) Garnavich & Karska 2006; (28) Nysewander et al. 2007; (29) Fynbo et al. 2006; (30) Mangano et al. 2007; (31) Melandri et al. 2006; (32) Quimby & Rykoff 2006; (33) Soyano et al. 2006; (34) Mundell et al. 2007; (35) Thoene et al. 2006; (36) Fynbo 2006; (37) Page et al. 2007; (38) Perley et al. 2008; (39) Thoene et al. 2007b; (40) Schmidt & Mackie 2007; (41) Thoene et al. 2007a; (42) Terra et al. 2007; (43) Sharapov et al. 2005; (44) Berger et al. 2006; (45) Efimov et al. 2006; (46) Malesani et al. 2007b.

TABLE 3

Swift Long GRBs with X-Ray Detections but No Optical Data at 11 hr

GRB	γ-ray Fluence[a] (10^{-7} erg cm^{-2})	γ-ray Fluence Error[a] (10^{-7} erg cm^{-2})	X-ray Integral Flux 0.3–10 keV @11 hr (10^{-13} erg cm^{-2} s^{-1})	X-ray Integral Flux Error[b] (10^{-13} erg cm^{-2} s^{-1})	X-ray Spectrum Photon Index	X-ray Spectrum Photon Index Lower Error	X-ray Spectrum Photon Index Upper Error	X-ray Flux Density[b] @3 keV @11 hr (10^{-13} μJy)	X-ray Flux Density Error[b] (10^{-13} μJy)
050124	11.9	0.66	12.4	2.7	1.89	0.22	0.27	51.3	14
050128	50.2	2.3	23.6	5.2	2	0.19	0.21	92.8	26
050215B	2.27	0.29	2.76	1.1	1.67	0.4	0.47	12.3	5.3
050219B	158	5	38.8	3.6	2.01	0.15	0.16	151	22
050223	6.36	0.65	1.28	0.53	1.9	0.51	0.62	5.26	2.7
050326	88.6	1.6	12.1	2.5	2.05	0.21	0.45	46.1	15
050505	24.9	1.8	31.1	3	2.03	0.085	0.089	120	15
050603	63.6	2.3	27.6	3.6	1.93	0.11	0.12	113	18
050607	5.92	0.55	2.13	0.65	2.49	0.5	0.59	5.67	4
050712	10.8	1.2	11	2.2	2.18	0.23	0.26	38.4	12
050713A	51.1	2.1	22	2.9	2.27	0.15	0.17	71.8	15
050713B	31.8	3.2	77.5	12	1.89	0.17	0.19	321	65
050714B	5.95	1	2.63	0.72	2.88	0.38	0.21	4.43	2.7
050716	61.7	2.4	9.57	1.7	2.16	0.25	0.29	33.9	10
050726	19.4	2.1	4.38	0.88	2.11	0.25	0.29	16.1	4.9
050814	20.1	2.2	10.2	1.7	2.01	0.14	0.15	40.1	8.6
050819	3.5	0.55	2.75	1.1	2.44	0.46	0.57	7.72	5.6
050822	24.6	1.7	17.9	2.3	2.21	0.15	0.16	61.1	12
050915A	8.5	0.88	3.63	0.89	1.93	0.33	0.43	14.8	5
050915B	33.8	1.4	5.74	1.9	2.21	0.3	0.37	19.7	9.3
051001	17.4	1.5	2.3	0.51	2.46	0.28	0.35	6.31	2.8
051008	50.9	1.4	9.78	1.6	2.16	0.19	0.2	34.6	8.6
051016B	1.7	0.22	11.9	2.4	1.86	0.19	0.21	49.7	13
051117A	43.4	1.6	5.96	1.1	2.36	0.18	0.21	18	5.3
051221A	11.5	0.35	7.52	1.4	2.12	0.17	0.19	27.5	6.9
060109	6.55	1	4.96	1	2.58	0.3	0.35	12	5.7
060111A	12	0.58	5.1	0.78	2.32	0.18	0.21	15.9	4.2
060111B	16	1.4	3.73	0.9	2.14	0.29	0.35	13.5	5
060115	17.1	1.5	5.66	2.3	2.72	0.46	0.68	11.6	10
060202	21.3	1.6	10.6	1.3	3.21	0.17	0.19	11.2	3.9
060204B	29.5	1.8	7.18	1.3	2.33	0.22	0.26	22.3	7
060211A	15.7	1.4	2.84	0.79	2.47	0.34	0.43	7.73	4.2
060306	21.3	1.2	11.7	1.5	2.28	0.15	0.17	37.8	8.1
060319	2.64	0.34	8.65	1.4	2.21	0.18	0.22	29.5	7.6
060428A	13.9	0.78	66	8	2.21	0.19	0.2	226	49
060428B	8.23	0.81	3.22	0.54	1.92	0.16	0.18	13.2	2.8
060507	44.5	2.3	7.85	1.6	2.14	0.21	0.25	28.4	8.3
060510A	80.5	3.1	178	21	1.98	0.069	0.14	708	100
060510B	40.7	1.8	1.45	0.5	2.32	0.36	0.5	4.54	2.6
060707	16	1.5	15.4	4.1	2.05	0.25	0.33	59	21
060708	4.94	0.37	7.5	1	2.05	0.12	0.12	28.6	5
060712	12.4	2.2	3.09	0.74	2.45	0.25	0.32	8.59	3.6
060719	15	0.91	5.93	1.2	2.77	0.27	0.33	11.5	5.6
060804	5.98	0.99	15.1	3.3	2.26	0.25	0.35	49.7	18

TABLE 3—*Continued*

GRB	γ-ray Fluence[a] (10^{-7} erg cm^{-2})	γ-ray Fluence Error[a] (10^{-7} erg cm^{-2})	X-ray Integral Flux 0.3–10 keV @11 hr (10^{-13} erg cm^{-2} s^{-1})	X-ray Integral Flux Error[b] (10^{-13} erg cm^{-2} s^{-1})	X-ray Spectrum Photon Index	X-ray Spectrum Photon Index Lower Error	X-ray Spectrum Photon Index Upper Error	X-ray Flux Density[b] @3 keV @11 hr (10^{-13} μJy)	X-ray Flux Density Error[b] (10^{-13} μJy)
060807	8.48	1.1	9.29	1.3	2.43	0.19	0.21	26.2	7.3
060813	54.6	1.4	43.2	11	2.16	0.33	0.36	154	61
060814	146	2.4	31.4	3.2	2.21	0.11	0.12	107	16
060923A	8.69	1.3	5.44	1	2.07	0.19	0.28	20.5	5.6
060923C	15.8	2.2	4.05	1	2.72	0.4	0.5	8.34	5.7
061004	5.66	0.31	2.06	0.67	2.4	0.53	0.67	6.04	4.2
061019	25.9	4	12.8	3	2.05	0.38	0.45	49	19
061222A	79.9	1.6	158	13	2.09	0.095	0.099	587	68
070103	3.38	0.46	0.951	0.21	2.06	0.27	0.29	3.62	1.1
070107	51.7	2.6	58	5.7	2.2	0.14	0.14	200	33
070129	29.8	2.7	16.5	4.6	2.14	0.22	0.25	59.5	22
070208	4.45	1	2.92	0.89	2.46	0.43	0.54	8.01	5.1
070220	104	2.3	7.26	1.5	1.7	0.23	0.27	32.2	7.7
070223	17	1.2	4.02	1.2	1.9	0.65	0.95	16.6	7.9
070306	53.8	2.9	77.8	11	2.18	0.16	0.18	273	60
070318	24.8	1.1	12.8	1.9	2.33	0.17	0.19	40	9.9
070328	90.6	1.8	45.6	5.5	2.03	0.14	0.16	176	30
070330	1.83	0.31	4.62	1.2	2.37	0.41	0.54	13.9	7.7
070420	140	4.5	53.9	5.2	2.04	0.16	0.17	207	32
070521	80.1	1.8	21.1	2.8	1.98	0.18	0.2	84	16
070529	25.7	2.4	3.73	0.87	2.18	0.26	0.4	13.1	4.9
070611	3.91	0.57	2.06	0.59	1.95	0.29	0.35	8.31	3.1
070616	192	3.5	8.41	1.6	2.49	0.24	0.3	22.3	8.7
070621	43	1	7.85	1.4	2.63	0.29	0.33	17.8	8.2
070704	59	3	6.69	1.8	1.97	0.35	0.58	26.7	11
070714A	1.5	0.2	1.53	0.53	2.42	0.73	0.95	4.36	3.8
070721A	0.71	0.18	1.43	0.45	2.65	0.39	0.39	3.17	2.1
070721B	36	2	3.5	0.72	1.88	0.18	0.17	14.6	3.7

[a] BAT prompt fluence in 15–150 keV band. Data from Sakamoto et al. (2008).
[b] XRT flux at 3 keV at 11 hr after the burst trigger. The error includes 10% systematic uncertainty.

TABLE 4
Correlation Fits and Coefficients

Data Set	Number of Data Points N	A[a]	B[a]	Correlation Coefficient r	Null Hypothesis Probability[b] $P_{\rm null}$	Fraction of Variability Due to Correlation[b] r^2
Long GRBs: Optical (y) vs. X-ray (x).....	37	1.62 ± 0.04	0.38 ± 0.03	0.44 ± 0.03	0.006	0.19
Short GRBs: Optical (y) vs. X-ray (x).....	6	0.72 ± 0.94	0.14 ± 0.45	0.06 ± 0.23	0.68	0.00
Long GRBs: X-ray (y) vs. γ-ray (x).....	111	2.11 ± 0.21	0.63 ± 0.04	0.53 ± 0.02	4×10^{-9}	0.28
Short GRBs: X-ray (y) vs. γ-ray (x).....	10	0.06 ± 1.07	0.36 ± 0.17	0.35 ± 0.14	0.31	0.12
Long GRBs: Fluence (y) vs. peak flux (x).....	218	-6.03 ± 0.01	0.83 ± 0.02	0.66 ± 0.01	4×10^{-29}	0.44
Short GRBs: Fluence (y) vs. peak flux (x).....	17	-7.06 ± 0.04	1.27 ± 0.06	0.84 ± 0.02	2×10^{-6}	0.71

[a] Fit with the function $y = 10^A x^B$.
[b] The significance of the correlation is $1 - P_{\rm null}$.

and 061006 ($\Delta m_R = 0.85$); the exceptions from Table 2 are 050713B ($\Delta m_R = 1.249$) and 070704 ($\Delta m_R = 5.014$). Corrections this large are highly uncertain due to the patchiness in extinction in the Galactic plane.

Our sample contains three GRBs with redshift values large enough ($z \simeq 4$) that Lyman blanketing may affect the R-band fluxes. For these bursts—050730, $z = 3.97$; 060206, $z = 4.05$; and 060210, $z = 3.91$—the expected redshifting of the Lyman series ($1 + z$) $\simeq 5$. For Lyα, 1215.7 Å $\rightarrow\sim$ 6080 Å, and for Ly∞, 911.3 Å $\rightarrow\sim$ 4560 Å. Thus, the effect of the redshifted absorption is to impact the blue edge of the R-band filter $\lambda_R \approx 6600 \pm 800$ Å. However, the R-band fluxes for the three highest z bursts (Fig. 1, *circles*) scatter about the mean R-band flux line, rather than being concentrated at low f_R values, as would have been expected had blanketing been an issue. Although for $z = 4$ the Lyα feature will be shifted redward of the ~6000 Å (skew-symmetric) peak of the R filter, the centroid and FWHM of the filter still predict that the bulk of the filter response lies redward of most of the Lyman series, which would be most dominant for $z = 4$ at $\lambda < 6000$ Å (e.g., for the Cousins [Bessell 90] $R_{\rm C}$ filter, $\lambda_{\rm eff} = 6588$, and $\Delta\lambda_{\rm FWHM} = 1568$ Å; Fukugita et al. 1995; see their Table 9). The absorptive effect would likely warrant a corrective multiplicative factor $\lesssim$1.5, which is small given the approximately five decade spread in log F_R for Figure 1. Therefore, we do not attempt to correct F_R for redshifted Lyman absorption for these three high-z bursts.

The gamma-ray fluences and peak fluxes are in the 15–150 keV band and are from the *Swift* Burst Alert Telescope (BAT; Barthelmy et al. 2005b), as compiled in the BAT GRB catalog (Sakamoto et al. 2008). For the gamma-ray flux needed in study 3, we use 1 s binning as quoted by Sakamoto et al. (2008).

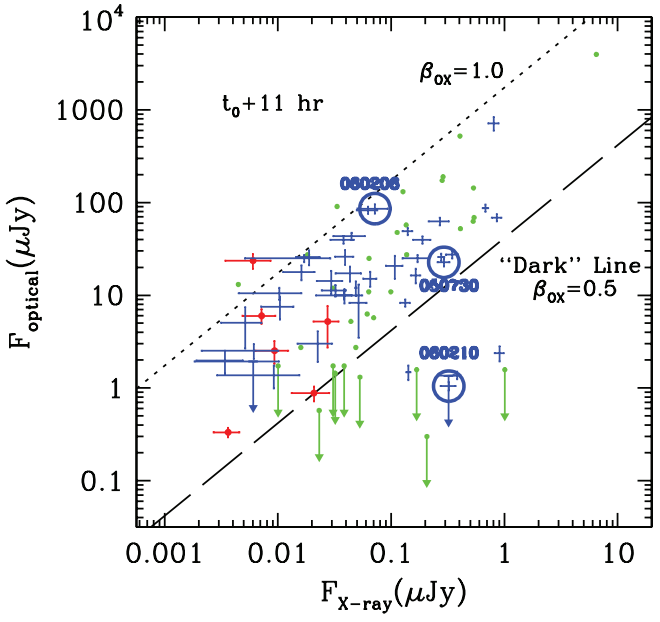

Fig. 1.—X-ray afterglow vs. optical afterglow flux densities of *Swift* short (*red symbols*) and long (*blue symbols*) GRBs at 11 hr after the burst. The three circled bursts are those for which $z > 3.9$. Also plotted are the pre-*Swift* GRBs (*green symbols*) taken from Jakobsson et al. (2004). For the Jakobsson et al. subsample with upper limits, we only plot those bursts for which the limiting magnitude is fainter than $m_R = 23$ (i.e., ~2 μJy). The XRT X-ray flux densities are at 3 keV, and the optical flux densities are in the R band (see Tables 1 and 2). Also shown is the dark burst separation line $\beta_{\rm OX} = 0.5$ (Jakobsson et al. 2004) and a line indicating $\beta_{\rm OX} = 1.0$.

2.4. *Correlation Analysis*

For each study, we have performed fits to the two-parameter correlation data using the Spearman rank test (Spearman 1904; Press et al. 1986) and derived the correlation coefficient, r, to determine the degree and significance of the correlation. Upper limits were not included in the fits. In the Spearman rank test, the probability of a null correlation, $P_{\rm null}$, is given by

$$P_{\rm null} = {\rm erfc}\left[r(N/2)^{1/2}\right], \quad (2)$$

where N is the number of data points. The significance of the correlation is $P_{\rm cor} = 1 - P_{\rm null}$. The fraction of the observed spread of the data that can be explained by the correlation is given by r^2. The fit parameters and correlation r values are listed in Table 4. Equation (2) only applies when N is large ($\gtrsim$10–20). For $N \simeq$ 1–10, the concept of applying a significance criterion to a correlation study begins to lose its meaning.[13] Therefore, although for completeness we list r and $P_{\rm null}$ values for cases with small N, we stress that they are only indicative of trends in those cases.

3. RESULTS

3.1. *X-Ray and Optical Afterglow Correlations*

Figure 1 shows the *Swift* X-ray afterglow average flux density at 3 keV as a function of the R-band optical flux density, both converted to μJy at 11 hr after the burst, for short and long bursts. The pre-*Swift* data points are taken from Jakobsson et al. (2004) and are shown as green symbols. Also shown (*dashed line*) is the constant X-ray–to–optical spectral index that they propose separates the true dark bursts from the rest. As listed in Table 4, the Spearman rank test for the two GRB populations in Figure 1 gives a null probability of ~0.01, or a 99% correlation probability between the optical and X-ray flux densities of the long GRBs, and only ~30% for the short population.

[13] This can be seen in the limit $N \rightarrow 2$, where one considers two data points, (x_1, y_1) and (x_2, y_2). In this example $r \equiv 1$, so the statement $r = 1$ carries no information and has no significance.

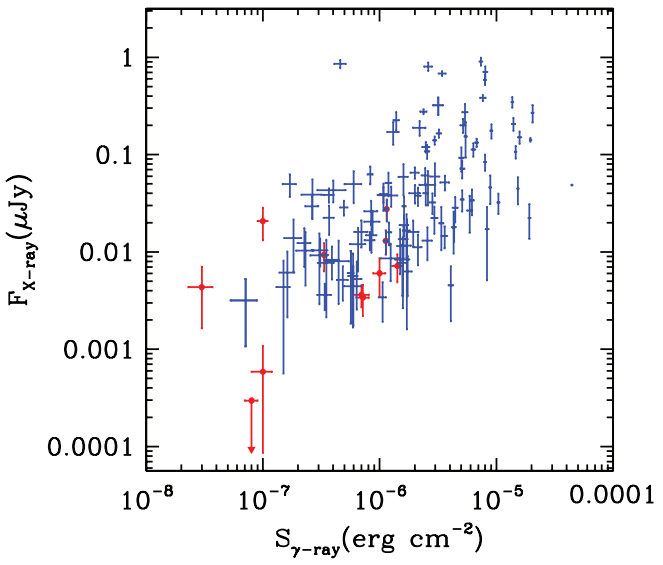

FIG. 2.—X-ray afterglow flux density vs. gamma-ray prompt fluence of *Swift* short (*red symbols*) and long (*blue symbols*) GRBs at 11 hr after the burst. The XRT X-ray flux densities are at 3 keV, and the BAT gamma-ray fluences are between 15 and 150 keV (Sakamoto et al. 2008). The XRT and BAT data are given in Tables 1–3.

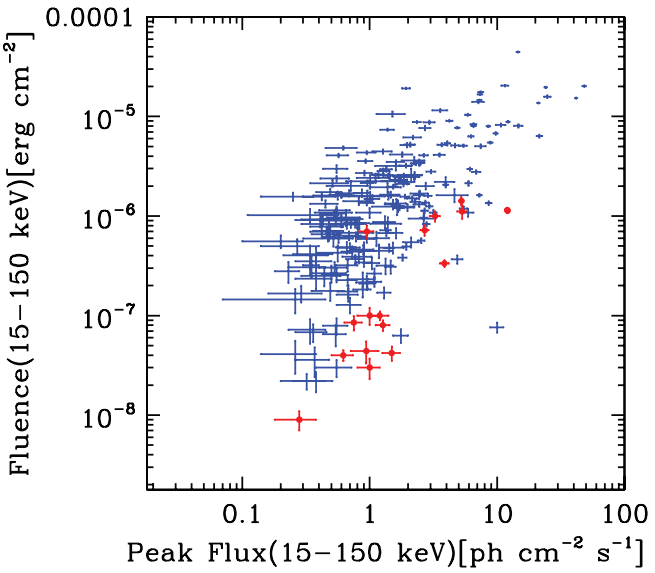

FIG. 3.—Prompt gamma-ray fluence vs. peak flux measured by BAT in the 15–150 keV band for all bursts through 2007 February (Sakamoto et al. 2008). Short bursts are shown by red symbols and long bursts by blue symbols.

The long *Swift* GRBs fall into the same general region of the plot as the pre-*Swift* ones. As with the pre-*Swift* bursts, several *Swift* long bursts (detections and upper limits) also fall below the Jakobsson et al. (2004) dark line. The brightest short GRBs fall in the midst of the long GRB points but in the region toward lower flux densities. To date there are no short bursts that fall below the dark burst line; those with low optical flux densities or upper limits tend to also have weak X-ray flux densities that place them above the line.

3.2. *Gamma-Ray Prompt and X-Ray Afterglow Correlations*

We show in Figure 2 the average X-ray afterglow flux density versus the gamma-ray fluence of the prompt emission for long and short *Swift* GRBs. We find a highly significant correlation (99.9999996% probability) for the long GRBs, albeit with a wide spread in the data. The correlation of the short bursts is less significant (69% probability), mostly due to the smaller number of points. There is an overlap between the brightest short bursts and the faintest long GRBs. The weakest short bursts are fainter than the weakest long bursts.

3.3. *Prompt Gamma-Ray Fluence and Peak Flux Correlations*

Figure 3 shows the prompt emission fluence as a function of peak flux for GRBs detected by BAT. We see a linear correlation for both short and long bursts with a significant spread in the correlation. The correlation probability is virtually 100% (null probability $= 2 \times 10^{-29}$) for long bursts and 99.9998% for short bursts. The best-fit lines are distinctly different for short and long bursts, with the long burst having a higher fluence, on average, for a given flux level than short bursts, as expected from duration alone.

4. DISCUSSION

4.1. *Correlations and Short/Long Distributions*

We show in this work that correlations exist between prompt and afterglow fluxes of GRBs and between different wavelength bands in the afterglow. The highest significance correlation is between the prompt emission gamma-ray fluence and the X-ray afterglow flux at a significance level of 99.9999996% for long bursts and 69% for short bursts. The correlation between the optical afterglow and X-ray afterglow fluxes is less significant at 99% significance for long bursts and only ~30% for short bursts (for a small sample, however).

It is important to note that there is a wide spread in the data for all of the correlations. The correlations are real and significant, but the fraction of the observed variations due to the correlations between the above parameters accounts for only a portion of the data spread. The correlation can only be used to predict a flux level to within approximately an order of magnitude. The fraction of the variation due to the correlations is given by the square of the correlation parameter r, which, as shown in Table 4, varies from a few percent to 50%. The rest of the data spread is due to other factors, such as correlations with additional unknown parameters. An example of an additional parameter is extinction in the optical afterglow.

Short bursts are weaker, on average, than long bursts in afterglow fluxes. There is overlap with the dimmer long bursts, but the short bursts extend to lower intensities than seen for long bursts. The average X-ray flux density at 3 keV at 11 hr for the short bursts is $\langle F_X(\text{short})\rangle = 9.6 \times 10^{-3}$ μJy, which is more than an order of magnitude less than the average for long bursts of $\langle F_X(\text{long})\rangle = 0.10$ μJy.

The X-ray–to–gamma-ray correlation in Figure 2 has a positive correlation with a slope of roughly unity. This suggests that brighter bursts have more kinetic energy in the afterglow phase to power the afterglow. This is a manifestation of similar radiative efficiency among different bursts and between long and short GRBs. Such a point was made by Zhang et al. (2007) based on an analysis of a smaller sample of early *Swift* GRBs.

Except for the bursts below the dark line, most bursts in Figure 1 are confined between lines with $\beta_{OX} = 0.5$ and 1.0. This is consistent with a general interpretation that the optical and X-ray emission belong to the same spectral component with an index close to 0.75. Within the standard model for emission via synchrotron radiation, for slow cooling which is generally relevant at $t = 11$ hr, one expects $\beta_{OX} \sim (p - 1)/2$ for

$\nu_m < \nu_O < \nu_X < \nu_c$, which has a typical value of 0.75 for the electron distribution power law $p = 2.5$. (An equivalent statement is that for this spectrum, the predicted ratio $F_R/F_X \approx 350$ yields a line intermediate between $\beta_{OX} = 0.5$ and 1.0 in Fig. 1.) This suggests that, on average, the cooling frequency is above or not much below the X-ray band at 11 hr.

4.2. *Dark GRBs*

Another comparison of short and long GRBs relates to dark bursts. Jakobsson et al. (2004; see also de Pasquale et al. 2003) used a simple criterion to define dark bursts as those with extremely low optical–to–X-ray afterglow ratios falling below the line of optical–to–X-ray spectral index β_{OX} equal to 0.5. It may seem counterintuitive that there can be dark bursts with optical detections and bursts not detected in the optical that are not dark, but the important criterion is how optically faint the burst is relative to its X-ray flux. For the pre-*Swift* sample there were five bursts with upper limits below the dark burst line (restricting the Jakobsson et al. sample to include only those with upper limits fainter than $m_R = 23$, or $\sim$2 μJy), compared to 24 bursts with actual measurements (not upper limits) above the line, giving a fraction of $\sim$17% in the dark category. For *Swift* there are two bursts with upper limits (GRB 050713B and 061222A) and three cases with measurements (GRB 060210, 070419B, and 070508) below the line compared with 34 long bursts above the line for a fraction of $\sim$17% in the dark category, the same as the pre-*Swift* sample. The conclusion is that *Swift* is sampling the same source environments as previous instruments.

The discovery of three cases of dark bursts with optical detections is particularly interesting. One possible concern with this finding is that *Swift* X-ray afterglow is contaminated in many bursts by emission components not from the external shocks, e.g., X-ray flares. In such instances, the Jakobsson et al. (2004) approach to define dark bursts is no longer relevant, since it assumes that the X-ray and optical emission is from the same emission component but separated by a cooling break. However, the X-ray light curves for the *Swift* dark bursts are smooth around 11 hr (and beyond the end of the X-ray plateau), with no significant contamination from other components. These are real dark bursts from both an observational and a physics perspective.

Correlation analyses between the optical and X-ray can help answer the question of whether these two afterglow components originate from the same physical processes. It is assumed in the Jakobsson et al. (2004) study that both X-ray and optical emission arise from the external forward shock. Multiwavelength observations in the *Swift* era reveal puzzling chromatic features of afterglow breaks (e.g., Panaitescu et al. 2006; Liang et al. 2007, 2008) that are not consistent with the simplest forward-shock model. Models invoking a non-forward-shock origin of X-ray afterglow have been discussed in the literature (e.g., Genet et al. 2007; Uhm & Beloborodov 2007; Ghisellini et al. 2007; Shao & Dai 2007; Panaitescu 2008). On the other hand, analyses suggest that the X-ray data are generally consistent with the temporal index and spectral index relations (e.g., Zhang & Mészáros 2004) predicted by the forward-shock models, although not in every case (Liang et al. 2007; Willingale et al. 2007). The optical/X-ray data of some bursts (e.g., Grupe et al. 2007; Mangano et al. 2007) are consistent with the same forward-shock model. Regardless of the exact process, the analysis presented in this paper shows that, generally, optical/X-ray afterglow fluxes are correlated, which suggests that they are due to the same emission process. The few cases well below the correlation line are found to be dark due to extinction in the host galaxy.

For the first time we can search for dark short bursts. No short bursts are seen that fall below the dark burst line. It is hard to find dark GRBs using this criterion, since X-ray afterglow fluxes are also low for the short bursts. However, there are some short bursts with bright X-ray afterglow, and, to date, none of those are seen to be highly deficient in optical afterglow. Statistics are still small, with only five optical detections, but if the observed trend continues we will be able to conclude that short bursts do not occur in regions with extremely high extinction, as is the case for some long bursts.

We are beginning to find optical detections of bursts below the dark burst line. In one of the three dark bursts with detections (GRB 060210), the burst is found to have high extinction associated with its host galaxy, explaining the low optical flux (Curran et al. 2007b). By modeling the differences between β_{opt}, β_X, and β_{OX} and taking into account the Lyα absorption ($z = 3.91$), Curran et al. find that the R-band source extinction could be 3.9 ± 0.7 mag ($\nu_c > \nu_O$) or 6.7 ± 0.6 mag ($\nu_c < \nu_O$). This is an important development in our understanding of dark GRBs. (For two of the three dark bursts with detections, 070419B and 070508, there has not yet been sufficiently detailed follow-up work on the putative hosts for constraints to be placed on the host extinction.) Assuming that the dark bursts can be largely explained by extinction, the optical–to–X-ray correlations, ignoring the dark bursts, will hold true. We note that new studies are being done to examine dark burst definitions (A. J. van der Horst et al. 2008, in preparation).

4.3. *Prompt Fluence and Flux Comparisons*

The comparison of fluences and peak fluxes in the prompt emission as shown in Figure 3 is a different kind of study than the two explained above. In this case, the strong observed correlation and high degree of separation of short and long bursts is expected; brighter bursts with higher peak fluxes naturally have higher fluences, and short bursts tend to have lower fluences for a given flux by the very fact of their short duration. Within the short and long classes, the spread in fluence that is seen for a given peak flux is due to the diversity of durations and spectral indices. Bursts with longer durations and hard spectra have higher fluences for the same peak flux.

It is interesting to note in Figure 3 that the short bursts tend to be fluence-limited in the BAT, while long bursts tend to be peak flux–limited. This is due to the way BAT operates. A valid GRB trigger requires a statistically significant excess in both the rate and image domains (McLean et al. 2004). The ability to form an image depends on the number of photons collected on various trigger timescales, which is related to the burst fluence. Even for relatively high peak fluxes, short bursts can have low fluence values and be limited in the number of photons available for the image trigger. On the other hand, long bursts tend to have higher fluences for a given peak flux and become rate-limited before the image limit is reached. BAT also has a pure-image mode for triggering where very long duration GRBs and other transients are found by comparing sky images instead of with a rate trigger. The lowest long-burst point in Figure 3, at a peak flux of $\sim$0.1, was such an image-mode trigger for the very long ($T90 =$ 35 minutes) and weak GRB 060218. A caveat on the above discussion is that the BAT trigger algorithm is complex, with $\sim$500 different trigger criteria evaluated. There are many different thresholds and limits coming into play for short and long burst triggering, with some mix of flux and fluence limits for both types.

This study was based on 1 s binning for the gamma-ray fluxes. We also investigated the effect of using a smaller bin size of

64 ms. Smaller bins pick out larger peak flux values when there is a short time structure or the burst has a duration shorter than the bin size. The effect of the smaller bin size is to shift the short bursts to the right (higher peak flux) relative to the long bursts by about a factor of 5. The larger bin size that we use allows for better statistics and is more reliable for long bursts. In either case, the short bursts tend to cluster toward lower fluences than the long bursts.

5. FUTURE PROSPECTS

The combined prompt and afterglow data set for *Swift* GRBs is the largest available to date. We have chosen a criterion of a solid measurement 11 hr after the burst for the afterglow measurements to be included in this study. Even with this stringent definition, there are more than 100 long bursts with X-ray afterglow data. The optical detections at 11 hr are less numerous, with about 40 good measurements, but still enough statistics for conclusions to be reached.

Short-burst correlation studies are now possible, and key results are beginning to emerge. The *Swift* database is growing quickly. In its expected lifetime of $\sim$10 yr, the mission should provide a sample of >40 short and >400 long GRBs with good afterglow and prompt observations. That size data set will allow more detailed correlation studies to investigate the interesting trends found in the current analysis.

The authors thank the following people for useful discussions: A. Fruchter, J. Fynbo, P. Jakobsson, A. Loeb, M. Nysewander, and E. Rol. We also acknowledge our anonymous referee, who provided excellent suggestions for improving the paper.

REFERENCES

Antonelli, L. A., et al. 2006, A&A, 456, 509
Barthelmy, S. D., et al. 2005a, Nature, 438, 994
———. 2005b, Space Sci. Rev., 120, 143
Berger, E. 2007, ApJ, 670, 1254
Berger, E., et al. 2005, Nature, 438, 988
———. 2006, GCN Circ. 5697, http://gcn.gsfc.nasa.gov/gcn/gcn3/5697.gcn3
———. 2007, ApJ, 664, 1000
Bikmaev, I., et al. 2005, GCN Circ. 3797, http://gcn.gsfc.nasa.gov/gcn/gcn3/3797.gcn3
Bloom, J. S., et al. 1999, Nature, 401, 453
———. 2006, ApJ, 638, 354
Burrows, D. N., et al. 2005, Space Sci. Rev., 120, 165
Butler, N. R. 2007, ApJ, 656, 1001
Cenko, S. B., et al. 2006, ApJ, 652, 490
Chen, H.-W., et al. 2007, ApJ, 663, 420
Cobb, B. E., & Bailyn, C. D. 2005, GCN Circ. 3104, http://gcn.gsfc.nasa.gov/gcn/gcn3/3104.gcn3
Curran, P. A., et al. 2007a, MNRAS, 381, L65
———. 2007b, A&A, 467, 1049
Dai, X., et al. 2007, ApJ, 658, 509
D'Avanzo, P., et al. 2006, GCN Circ. 5884, http://gcn.gsfc.nasa.gov/gcn/gcn3/5884.gcn3
Della Valle, M., et al. 2006, ApJ, 642, L103
de Pasquale, M., et al. 2003, ApJ, 592, 1018
———. 2006, A&A, 455, 813
Durig, D. T., & Price, A. 2005, GCN Circ. 4023, http://gcn.gsfc.nasa.gov/gcn/gcn3/4023.gcn3
Efimov, Yu., et al. 2006, GCN Circ. 5986, http://gcn.gsfc.nasa.gov/gcn/gcn3/5986.gcn3
Eichler, D., Livio, M., Piran, T., & Schramm, D. N. 1989, Nature, 340, 126
Firmani, C., Ghisellini, G., Avila-Reese, V., & Ghirlanda, G. 2006, MNRAS, 370, 185
Fox, D. B., et al. 2005, Nature, 437, 845
Fukugita, M., Shimasaku, K., & Ichikawa, T. 1995, PASP, 107, 945
Fynbo, J. P. U. 2006, GCN Circ. 5818, http://gcn.gsfc.nasa.gov/gcn/gcn3/5818.gcn3
Fynbo, J. P. U., et al. 2006, Nature, 444, 1047
———. 2007, preprint (astro-ph/0703458)
Galama, T. J., et al. 1998, Nature, 395, 670
Garnavich, P., & Karska, A. 2006, GCN Circ. 5253, http://gcn.gsfc.nasa.gov/gcn/gcn3/5253.gcn3
Gehrels, N., et al. 2004, ApJ, 611, 1005
———. 2005, Nature, 437, 851
Genet, F., Daigne, F., & Mochkovitch, R. 2007, MNRAS, 381, 732
George, K., Banerjee, D. P. K., Chandrasekhar, T., & Ashok, N. M. 2006, ApJ, 640, L13
Ghirlanda, G., Nava, L., Ghisellini, G., & Firmani, C. 2007, A&A, 466, 127
Ghisellini, G., Ghirlanda, G., Nava, L., & Firmani, C. 2007, ApJ, 658, L75
Grupe, D., et al. 2007, ApJ, 662, 443
Hjorth, J., et al. 2003, Nature, 423, 847
———. 2005, Nature, 437, 859
Huang, K. Y., et al. 2007, ApJ, 654, L25
Jakobsson, P., et al. 2004, ApJ, 617, L21
Kamble, A., Resmi, L., & Misra, K. 2007, ApJ, 664, L5
Kouveliotou, C., Meegan, C. A., Fishman, G. J., Bhat, N. P., Briggs, M. S., Koshut, T. M., Paciesas, W. S., & Pendleton, G. N. 1993, ApJ, 413, L101
Kulkarni, S. R. 2005, preprint (astro-ph/0510256)
Lattimer, J. M., & Schramm, D. N. 1974, ApJ, 192, L145
Li, L.-X., & Paczyński, B. 1998, ApJ, 507, L59
Liang, E.-W., Racusin, J. L., Zhang, B., Zhang, B.-B., & Burrows, D. N. 2008, ApJ, 675, 528
Liang, E.-W., Zhang, B.-B., & Zhang, B. 2007, ApJ, 670, 565
MacFadyen, A. I., & Woosley, S. E. 1999, ApJ, 524, 262
Malesani, D., Stella, L., Covino, S., Lidman, C., & Naef, D. 2006, GCN Circ. 5705, http://gcn.gsfc.nasa.gov/gcn/gcn3/5705.gcn3
Malesani, D., et al. 2007a, A&A, 473, 77
———. 2007b, GCN Circ. 6674, http://gcn.gsfc.nasa.gov/gcn/gcn3/6674.gcn3
Mangano, V., et al. 2007, A&A, 470, 105
McLean, K. M., Fenimore, E. E., Palmer, D., Barthelmy, S., Gehrels, N., Krimm, H., Markwardt, C., & Parsons, A. 2004, in AIP Conf. Proc. 727, Gamma-Ray Bursts: 30 Years of Discovery, ed. E. E. Fenimore & M. Galassi (Melville: AIP), 667
Melandri, A., Tanvir, N., & Guidorzi, C. 2006, GCN Circ. 5322, http://gcn.gsfc.nasa.gov/gcn/gcn3/5322.gcn3
Mészáros, P., & Rees, M. J. 1997, ApJ, 476, 232
Milne, P. A. 2006, GCN Circ. 5127, http://gcn.gsfc.nasa.gov/gcn/gcn3/5127.gcn3
Misra, K., & Pandey, S. B. 2005, GCN Circ. 3396, http://gcn.gsfc.nasa.gov/gcn/gcn3/3396.gcn3
Misra, K., et al. 2007, A&A, 464, 903
Mochkovitch, R., Hernanz, M., Isern, J., & Martin, X. 1993, Nature, 361, 236
Monfardini, A., et al. 2006, ApJ, 648, 1125
Mundell, C. G., et al. 2007, ApJ, 660, 489
Nava, L., Ghisellini, G., Ghirlanda, G., Tavecchio, F., & Firmani, C. 2006, A&A, 450, 471
Nousek, J. A., et al. 2006, ApJ, 642, 389
Nysewander, M., Fruchter, A. S., & Pe'er, A. 2008, ApJ, submitted (arXiv: 0806.3607v1)
Nysewander, M., et al. 2007, ApJ, submitted (arXiv: 0708.3444v2)
Oates, S. R., et al. 2006, MNRAS, 372, 327
Oechslin, R., Janka, H.-T., & Marek, A. 2007, A&A, 467, 395
Paczyński, B. 1986, ApJ, 308, L43
Page, K. L., et al. 2007, ApJ, 663, 1125
Panaitescu, A. 2008, MNRAS, 383, 1143
Panaitescu, A., et al. 2006, MNRAS, 366, 1357
Pandey, S. B., et al. 2006, A&A, 460, 415
Perley, D. A., Thoene, C. C., & Bloom, J. S. 2007, GCN Circ. 6774, http://gcn.gsfc.nasa.gov/gcn/gcn3/6774.gcn3
Perley, D. A., et al. 2008, ApJ, 672, 449
Pian, E., et al. 2006, Nature, 442, 1011
Piran, T., Kumar, P., Panaitescu, A., & Piro, L. 2001, ApJ, 560, L167
Press, W. H., Flannery, B. P., Teukolsky, S. A., & Vetterling, W. T. 1986, Numerical Recipes (New York: Cambridge Univ. Press)
Price, P. A., et al. 2006, GCN Circ. 5077, http://gcn.gsfc.nasa.gov/gcn/gcn3/5077.gcn3
Quimby, R., & Rykoff, E. S. 2006, GCN Circ. 5377, http://gcn.gsfc.nasa.gov/gcn/gcn3/5377.gcn3
Rol, E., et al. 2005, ApJ, 624, 868
———. 2007, ApJ, 669, 1098

Roming, P. W. A., et al. 2005, Space Sci. Rev., 120, 95
———. 2006, ApJ, 652, 1416
Rosswog, S., Ramirez-Ruiz, E., & Davies, M. B. 2003, MNRAS, 345, 1077
Rykoff, E. S., et al. 2006, ApJ, 638, L5
Sakamoto, T., et al. 2008, ApJS, 175, 179
Salmonson, J. D., & Galama, T. J. 2002, ApJ, 569, 682
Schlegel, D. J., Finkbeiner, D. P., & Davis, M. 1998, ApJ, 500, 525
Schmidt, B., & Bayliss, D. 2006, GCN Circ. 4880, http://gcn.gsfc.nasa.gov/gcn/gcn3/4880.gcn3
Schmidt, B., & Mackie, G. 2007, GCN Circ. 6325, http://gcn.gsfc.nasa.gov/gcn/gcn3/6325.gcn3
Shao, L., & Dai, Z. G. 2005, ApJ, 633, 1027
———. 2007, ApJ, 660, 1319
Sharapov, D., et al. 2005, GCN Circ. 3701, http://gcn.gsfc.nasa.gov/gcn/gcn3/3701.gcn3
Soderberg, A. M., et al. 2006, ApJ, 650, 261
———. 2007, ApJ, 661, 982
Sollerman, J., et al. 2007, A&A, 466, 839
Soyano, T., Mito, H., & Urata, Y. 2006, GCN Circ. 5548, http://gcn.gsfc.nasa.gov/gcn/gcn3/5548.gcn3
Spearman, C. 1904, Am. J. Psychol., 15, 72
Stanek, K. Z., et al. 2003, ApJ, 591, L17
Stanek, K. Z., et al. 2007, ApJ, 654, L21
Stratta, G., Fiore, F., Antonelli, L. A., Piro, L., & de Pasquale, M. 2004, ApJ, 608, 846
Terra, F., et al. 2007, GCN Circ. 6458, http://gcn.gsfc.nasa.gov/gcn/gcn3/6458.gcn3
Thoene, C. C., Fynbo, J. P. U., & Jakobsson, P. 2006, GCN Circ. 5747, http://gcn.gsfc.nasa.gov/gcn/gcn3/5747.gcn3
Thoene, C. C., Fynbo, J. P. U., & Williams, A. 2007a, GCN Circ. 6389, http://gcn.gsfc.nasa.gov/gcn/gcn3/6389.gcn3
Thoene, C. C., Kann, D. A., Augusteijn, T., & Reyle-Laffont, C. 2007b, GCN Circ. 6154, http://gcn.gsfc.nasa.gov/gcn/gcn3/6154.gcn3
Uhm, Z. L., & Beloborodov, A. M. 2007, ApJ, 665, L93
Villasenor, J. S., et al. 2005, Nature, 437, 855
Willingale, R., et al. 2007, ApJ, 662, 1093
Woosley, S. E. 1993, ApJ, 405, 273
Woosley, S. E., & Bloom, J. S. 2006, ARA&A, 44, 507
Woźniak, P. R., Vestrand, W. T., Wren, J. A., White, R. R., Evans, S. M., & Casperson, D. 2005, ApJ, 627, L13
Yost, S. A., et al. 2007, ApJ, 657, 925
Zhang, B., & Mészáros, P. 2004, Int. J. Mod. Phys. A, 19, 2385
Zhang, B., et al. 2006, ApJ, 642, 354
———. 2007, ApJ, 655, 989